Threshold switching mechanism by high-field energy gain in the hopping transport of chalcogenide glasses

Daniele Ielmini*
Dipartimento di Elettronica e Informazione, Politecnico di Milano and IUNET, piazza L. da Vinci 32, I-20133 Milano, Italy
(Received 7 February 2008; revised manuscript received 3 June 2008; published 8 July 2008)

Chalcogenide glasses are widely used in phase-change nonvolatile memories and in optical recording media for their ability to rapidly change their structure to crystalline, thus obtaining different electrical resistance and optical reflectivity. Chalcogenide glasses universally display *threshold switching*, that is a sudden, reversible transition from a high-resistivity state to a low-resistivity state observed in the current-voltage (*I-V*) characteristic. Since threshold switching controls the operating voltage and speed of phase-change memories, the predictability of the switching voltage, current, and speed is of critical importance for selecting the proper chalcogenide material for memory applications. Although threshold switching has long been recognized to be an electronic process with an intimate relation to localized states, its detailed physical mechanism is still not clear. In this work, threshold switching is explained by the field-induced energy increase in electrons in their hopping transport, moderated by the energy relaxation due to phonon-electron interaction. The energy increase leads to an enhancement of conductivity and a collapse of the electric field within the amorphous chalcogenide layer, accounting for the observed negative differential resistance at switching. Threshold switching is found to obey to a constant electrical-power condition. The proposed model generally applies to low-mobility semiconductors featuring a deep Fermi level and hopping-type conduction, and can predict the thickness, temperature, and material dependence of threshold voltage and current.

DOI: 10.1103/PhysRevB.78.035308 PACS number(s): 72.20.Ht, 72.80.Ng, 73.61.Jc

I. INTRODUCTION

Chalcogenide glasses are attracting a growing research interest for their broad application as phase-change materials in nonvolatile memories and optical recording media.[1,2] The most intriguing phenomenon in the conduction characteristic of these materials is threshold switching. First discovered in chalcogenide glasses by Ovshinsky[3] in the late 1960s, threshold switching is the result of a negative differential-resistance (NDR) behavior and appears as a sudden transition to a highly conductive state, once the applied electrical voltage exceeds a critical (threshold) voltage.[4] In phase-change memories, threshold switching defines the critical boundary between the read and write ranges for current and voltage,[5] while the switching dynamics determines the ultimate speed for programming the memory cell.[4] Therefore, the ability to predict the threshold switching voltage and speed for a specific chalcogenide material is essential for developing fast and reliable phase-change memories.[5]

Understanding the threshold switching mechanism is an essential task not only in view of the industrial application, but also in the fundamental study of band structure and transport properties of amorphous semiconductors.[6–8] In fact, the nature of threshold switching was recognized to be electronic,[3,9,10] and the essential role of trapped-carrier transport, namely small-polaron hopping[11–14] or thermally induced Poole-Frenkel (PF) conduction,[15,16] was pointed out. A detailed physical description of threshold switching may thus contribute to the conceptual clarification of transport mechanisms at localized states in amorphous semiconductors, particularly under off-equilibrium conditions.[17–19]

The present study is a theoretical analysis of conduction and threshold switching in chalcogenide glasses based on (a) thermally assisted hopping transport,[15,16] (b) enhancement of carrier energy at high electric field,[16–19] and (c) energy-relaxation phenomena due to electron-phonon interaction.[17–19] First, the thermally assisted hopping conduction model in chalcogenide glasses is clarified with the aid of numerical simulations to compare tunneling and thermally activated PF transport contributions. Then a physical model for threshold switching is developed based on the balance between field-induced energy gain and energy relaxation by electron-phonon scattering. The model accounts for the thickness, temperature, and energy-gap dependence of subthreshold and switching characteristics of chalcogenide glasses.

II. THERMALLY ASSISTED HOPPING

The electronic threshold switching in chalcogenide glasses is interpreted here as a result of an instability in the transport process at high electric fields. Thus, to develop a realistic switching model, it is necessary to understand electrical transport at equilibrium in the chalcogenide glass. Chalcogenide materials in the amorphous phase are characterized by the presence of a large concentration of localized states (or traps) for electrons and holes in the forbidden gap, as a result of the disordered atomic structure at long range.[6,8,20] Given the large concentration of donor and acceptor states, the Fermi level tends to locate in the middle of the energy gap, leading to a large resistivity and a large activation energy for conduction.[15,20] Since the density of states is significant at the Fermi level, electrical conduction is controlled by trap states.[20] This has been evidenced by experiments on amorphous $Ge_2Sb_2Te_5$, a typical chalcogenide material used in phase-change memory applications.[15] The current in $Ge_2Sb_2Te_5$ devices was shown to increase exponentially with voltage, and the activation energy for conduc-

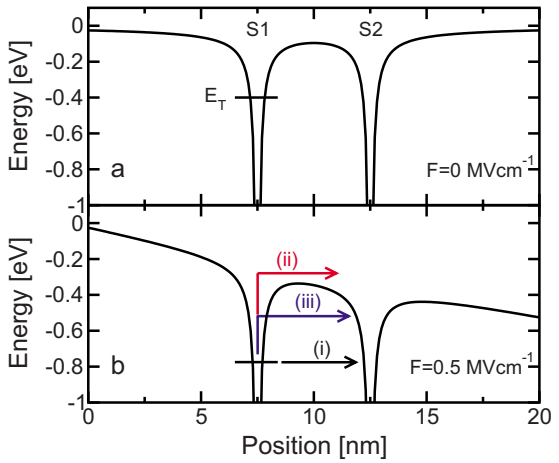

FIG. 1. (Color online) Profile of the electron potential energy along the minimum path between localized states S1 and S2, with electric field F = 0 (top) and 0.5 MV cm^{-1} (bottom). Schematic for the electron transport processes via localized states: (i) tunneling through the energy barrier at E_T, (ii) thermal (PF) emission over the energy barrier and (iii) thermally assisted tunneling through the energy barrier at an energy $E > E_T$.

tion was found to be close to half of the energy gap and linearly decreasing with voltage. These data were interpreted as consequences of a trap-limited transport process, e.g., *hopping* of carriers through localized states by the fundamental mechanisms of tunneling and/or PF effects.[15,16] Moreover, a hopping mechanism due to small polarons was evidenced by Hall measurements for some chalcogenide glasses, namely As_2Te_3, As_2Se_3, and Sb_2Te_3.[12–14] In these cases, carriers hop through localized states resulting from self-trapping in the disorder network, rather than through pre-existing gap states associated to point defects (dangling bonds, vacancies, etc.) or to the structural and chemical disorder (i.e., the so-called Anderson states[20]). In general, the hopping process may occur at defects- and disorder-related states, although carrying a significant small-polaron contribution due to the distortion/relaxation of the local structure when a hopping carrier is captured/emitted.[20] It should be noted that whether the localized states are due to small polarons or to disorder or to both, the transfer of a carrier from one state to the other occurs by the same fundamental processes, namely thermal emission or tunneling. The only difference is that, in the case of a polaron contribution to localized state, the activation energy for transport includes both the thermal emission for the carrier hopping and the structural rearrangement in the vicinity of the trapped carrier. However, the functional dependence on temperature and voltage of the hopping process will not be affected by the original assumption about the nature of the localized state.

The tunneling and thermal-emission mechanisms are depicted in Fig. 1, showing the energy-potential profile along the direction connecting two positively charged states, S1 and S2. No electric field is applied in Fig. 1(a), while a field $F=0.5$ MV cm^{-1} is assumed in Fig. 1(b). The localized states are assumed to have an energy of $E_T=E_C-0.3$ eV at zero applied field, where E_C is the conduction-band edge in the middle between the two traps. These were assumed to be located at a distance $\Delta z=5$ nm from each other. As shown in Fig. 1(b), the tunneling mechanism (i) occurs by transmission through the potential barrier from S1 to S2, while PF transport (ii) requires that the electron is thermally emitted to E_C, i.e., the first available state extending freely from S1 to S2. After the electron accesses the level E_C, recapture by the S2 will be possible. Also shown in Fig. 1(a) is a third mechanism (iii), obtained by a combination of thermal emission and tunneling, namely thermally assisted tunneling. This consists of a thermal excitation within S1 to an energy level *E below* E_C, followed by tunneling through the potential barrier seen at E. While the probability of reaching E is exponentially decreasing with E, the probability of tunneling through the barrier may be significantly higher than the tunneling probability for a "cold" electron at E_T.

To assess the nature of the conduction mechanism in chalcogenide glasses, the energy dependence of the average transfer rate from S1 to S2 was calculated. In the calculations, the transfer rate $R[s^{-1}\ \mathrm{eV}^{-1}]$ was evaluated as

$$R(E) = \frac{P_{\mathrm{tun}}(E)}{\tau_0}\frac{\mathrm{dP}_e}{\mathrm{dE}}, \tag{1}$$

where τ_0 is a characteristic attempt-to-escape time for electron excitation in the localized state, dP_e is the probability for an electron to have an energy between E and $E+\mathrm{dE}$, and P_{tun} is the tunneling probability at E. The attempt-to-escape time was set to $\tau_0=10^{-14}$ s, consistent with the typical phonon-induced excitation time (10^{-14}–10^{-13} s).[20] $\mathrm{dP}_e/\mathrm{dE}$ was assumed to obey a Maxwell-Boltzmann distribution, thus neglecting the effects of energy quantization in the potential wells. $P_{\mathrm{tun}}(E)$ was calculated according to the Wentzel-Kramers-Brillouin (WKB) approximation and considering the potential barrier across the minimum path from S1 to S2, as shown in Fig. 1. For electron energies above the potential barrier top [$E > E_C$ in Eq. (1)], a unit tunneling probability was assumed ($P_{\mathrm{tun}}=1$). The energy $E_T=E_C-0.3$ eV roughly corresponds to typical trap energy levels located close to the Fermi level for materials used in phase-change memory applications, e.g., amorphous $Ge_2Sb_2Te_5$.

Figure 2 shows the electron transfer rate calculated by Eq. (1), as a function of energy, for electric fields $F=0$, 0.1, and 0.2 MV cm^{-1} at room temperature. Larger rates in the figure correspond to higher current contributions. The results indicate that tunneling at $E=E_T$ (i.e., without excitation) is practically negligible, as compared to thermally assisted tunneling ($E_T < E < E_C$) and PF emission ($E \geq E_C$). The transfer rate is maximum for energies around the top of the barrier (E_c for $F=0$): This is because Eq. (1) features the product of P_e, which *decreases* for increasing E, and P_{tun}, which *increases* for increasing E. The overall contributions of thermally assisted tunneling and PF are thus comparable for typical trap energies in chalcogenide glasses.

To discriminate between tunneling and PF contributions in chalcogenide transport, the dependence of tunneling time τ_{tun} and PF time τ_{PF} on applied electric field F and temperature T was studied. Transfer times τ_{tun} and τ_{PF} represent the average time for an electron to be transferred from S1 to S2 by thermally assisted tunneling and PF emission, respectively. The transfer times were calculated as $[\int R(E)\mathrm{dE}]^{-1}$,

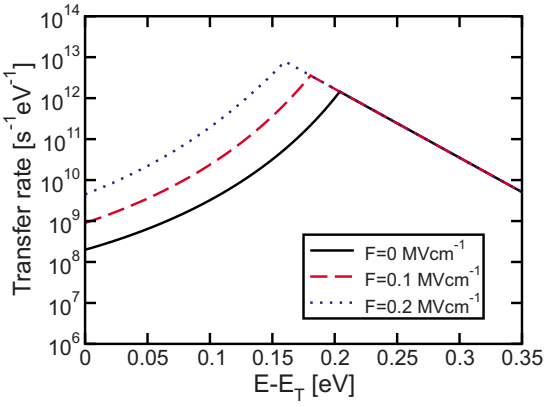

FIG. 2. (Color online) Transfer rates for the transport mechanisms considered in Fig. 1, as a function of the energy measured with respect to the trap level E_T. A trap energy $E_T=E_C-0.3$ eV was used. Rates were calculated for three values of the electric field by Eq. (1).

where the integral was evaluated in the energy ranges (E_T, E_C) and (E_C, ∞) for τ_{tun} and τ_{PF}, respectively. The distribution function P_e was normalized to unity [$\int P_e(E)dE=1$]. Figure 3 shows the calculated transfer times as a function of voltage and for a constant temperature $T=300$ K, while Fig. 4 shows the calculated times as a function of $(\text{kT})^{-1}$ and for a constant electric field $F=0.2$ MV cm^{-1}. The figures also include the total transfer time $\tau_{\text{tot}}=\tau_{\text{tun}}\tau_{\text{PF}}/(\tau_{\text{tun}}+\tau_{\text{PF}})$. Both τ_{tun} and τ_{PF} decrease exponentially with F in Fig. 3 and increase exponentially (Arrhenius dependence) with $(\text{kT})^{-1}$ in Fig. 4, as experimentally observed in Ref. 15. Note in Fig. 3 that τ_{PF} displays an exponential dependence on F, instead of $F^{1/2}$ of the conventional PF mechanism:[19] This is because the potential barrier lowering increases linearly with F for very short distances among traps $\Delta z \leq 5$ nm (i.e., Poole behavior[16,19]). For relatively large $\Delta z > 10$ nm, the conventional PF regime is recovered.[16,21] Figure 3 also compares calculated times for different trap energies, in the range from 0.2 to 0.4 eV below E_C: No significant variation in the relative amount of τ_{tun} and τ_{PF} and their field dependence is seen. The inset of Fig. 4

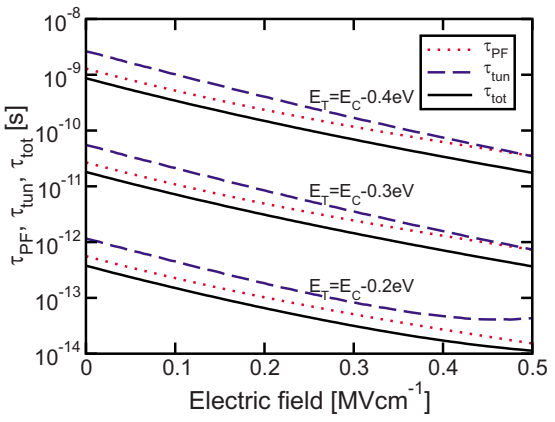

FIG. 3. (Color online) Calculated transfer times τ_{PF}, τ_{tun}, and τ_{tot} as a function of the electric field at room temperature. Trap energies E_T-E_C=−0.2, −0.3, and −0.4 eV were used.

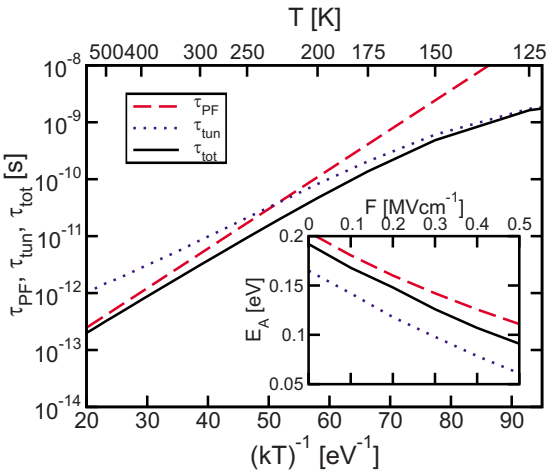

FIG. 4. (Color online) Calculated transfer times τ_{PF}, τ_{tun}, and τ_{tot} as a function of $(\text{kT})^{-1}$. A trap energy $E_T=E_C-0.2$ eV with an electric field $F=0.2$ MV cm^{-1} was used. The inset shows the activation energies E_A, i.e., the slopes of τ_{PF}, τ_{tun}, and τ_{tot} in the Arrhenius plot, as a function of the applied electric field F.

shows the F dependence of the activation energy E_A (i.e., slope on the Arrhenius plot) for the calculated τ_{tun}, τ_{PF}, and τ_{tot}: E_A decreases linearly with electric field, which is another distinctive feature of the experimentally observed trap-limited transport in chalcogenide glasses.[15]

From the comparison in Figs. 2–4, we conclude that both the magnitude and the field/temperature dependence of tunneling and PF processes in the trap-limited current are comparable, at least in the range of temperature, field, energy, and trap spacing of interest for typical chalcogenide materials used in memory applications. The common feature in these two processes as seen in Fig. 4 is however their *thermal activation*, namely the need for a significant energy excitation (e.g., by electron-phonon interaction) for a successful tunneling through or emission over the potential barrier. We will refer to this combined mechanism as a *thermally assisted hopping* in the following. Hopping for electrons will be described as a thermal emission mechanism over an *effective* energy barrier, which is obtained replacing the conduction-band level E_C with a conduction-band mobility edge E_C'. Hole-hopping mechanism can be described similarly, replacing the valence-band edge E_V with the corresponding mobility edge E_V'. This substitution allows taking into account the thermally assisted tunneling contribution occurring at energies below E_C. As already mentioned, the activation energy in the case of small-polaron hopping includes not only the carrier energy required to overcome the hopping barrier, but also the energy for the network relaxation associated to carrier self-trapping.

Thermally assisted hopping current density J can be written referring to the pictorial energy diagram in Fig. 5(a), indicating the conduction and valence mobility edges (E_C' and E_V', respectively), and the equilibrium Fermi level E_{F0}. For electron hopping, J is given by[16]

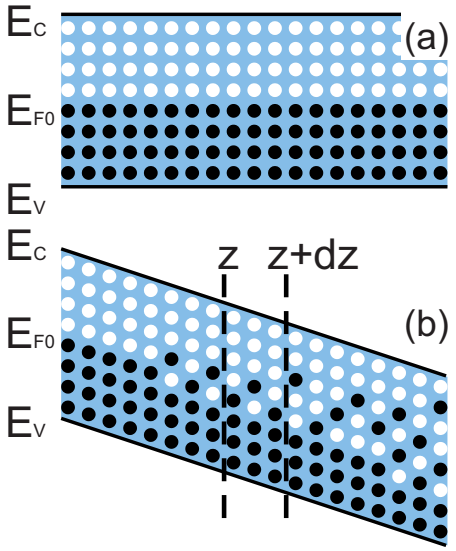

FIG. 5. (Color online) (a) schematic for the energy distribution of electrons in the amorphous chalcogenide film at equilibrium (no applied electrical field). The mobility edges at the conduction and valence bands E'_C and E'_V, respectively, and the Fermi level E_{F0} are shown. Black and white circles schematically represent occupied and unoccupied localized states. (b) is the same as (a) but under off-equilibrium conditions at high electric field. Note the increase in average energy E_F.

$$J = 2qN_T\frac{\Delta z}{\tau_0}e^{-\frac{E'_C-E_{F0}}{kT}}\sinh\left(\frac{qF\Delta z}{2kT}\right), \tag{2}$$

where q is the elementary charge, N_T [in units (cm^{-3})] is the density of traps between E_{F0} and E'_C, i.e., those contributing to the electron current, and Δz is the average distance between localized states. The hopping current density in Eq. (2) includes both PF emission and thermally assisted tunneling to a neighbor trap, as already discussed. The states involved in the hopping process may result from small polarons[11–14] or from defects and disorder in the glassy network,[6,8,15,20] or from both.[20] The exponential dependence on $(E'_C-E_{F0})/kT$ represents the thermal-excitation probability from the average electron energy (E_{F0}) to the mobility edge E'_C.[16,20] The sinh function in Eq. (2) results from the net sum of the exponential current densities flowing parallel and opposite to the electric field, respectively.[16,19,20]

Equation (2) was checked against electrical characterization results for nanometer-sized regions of amorphous $Ge_2Sb_2Te_5$ with thickness in the range of few tens of nanometers.[15,16] The equation could account for several experimental observations in the current/voltage regime below threshold switching, namely (a) the voltage dependence of the current, comprising a linear and an exponential regime, (b) the Arrhenius-like temperature dependence of the current, (c) the voltage dependence of the activation energy for conduction, and (d) the correlation between low-voltage resistance and the logarithmic subthreshold slope, defined as $d\log(J)/dV$.[16] This broad agreement with experimental results supports the equilibrium-transport model in Eq. (2) as a sound theoretical basis to investigate the threshold switching mechanism.

III. THRESHOLD SWITCHING MECHANISM

Threshold switching in chalcogenide glasses appears as a sudden increase in conductivity with a NDR behavior, leading to a characteristic snap back of the voltage. To account for this current-instability phenomenon, the effects of high electric fields on the thermally assisted hopping mechanism are studied. Figure 5(a) schematically shows the mobility gap of a chalcogenide glass,[20] defined by mobility edges E'_C and E'_V, and where the equilibrium Fermi level E_{F0} is pinned at midgap.[22] Application of a large voltage can lead to an energy gain of the carriers by the electric field, thus establishing a nonequilibrium carrier distribution in the amorphous semiconductor as depicted in Fig. 5(b).[16–19,23] Considering only electron transport for simplicity, the *average excess energy* for electrons at one point z along the transport direction can be given by the difference between the quasi-Fermi energy E_F, defined as the energy level for which the state-filling probability is 1/2, and E_{F0}. The off-equilibrium electron distribution may be equivalently described by the increased effective electron temperature over the equilibrium temperature T, although the E_F-based description is preferred here for simplicity.

While the electric field tends to raise E_F, inelastic scattering processes reduce the excess energy. The effect of inelastic scattering can be modeled as a first-order energy relaxation rate, given by[17–19]

$$\left.\frac{dE_F}{dt}\right|_{loss} = -\frac{E_F-E_{F0}}{\tau_{rel}}, \tag{3}$$

where the energy relaxation time τ_{rel} can be associated to electron-phonon interaction at localized states.[20] The balance between energy gain and relaxation in the slice between z and $z+dz$ shown in Fig. 5(b) thus reads

$$\frac{J(z)E_F(z)}{q} - \frac{J(z+dz)E_F(z+dz)}{q} + J(z)F(z)dz - \frac{E_F-E_{\{F0\}}}{\tau_{rel}}n_T(z)dz = 0. \tag{4}$$

In Eq. (4), the first and second terms on the left hand side are the product of J and the average excess energy E_F, divided by the unit charge q, and account for the energy flow into the slice at z and out from the slice at $z+dz$, respectively, in units [J $cm^{-2}s^{-1}$]. The third and fourth terms represent energy gain and loss [from Eq. (3)], respectively, where the concentration of trapped electrons n_T contributing to the electron current is used. The trapped electron concentration can be obtained by the density of states as

$$n_T = N_T\frac{kT}{E'_C-E_{F0}}, \tag{5}$$

where it is assumed that the trap distribution N_T is uniform in energy and that only traps within an energy range kT are populated, which is equivalent to integrating the exponentially decreasing Maxwell-Boltzmann distribution.[20] In Eq. (4), J is uniform due to the continuity condition $[J(z)=J(z+dz)]$, thus the equation can be simplified to obtain

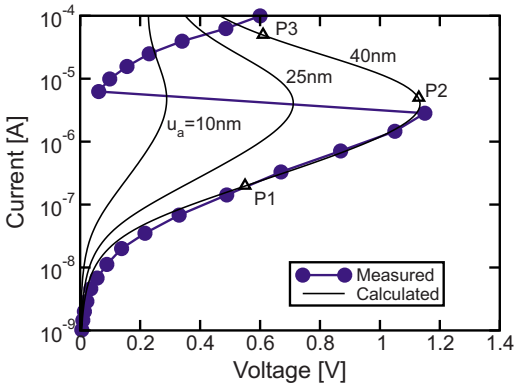

FIG. 6. (Color online) Measured *I-V* curve for a phase-change memory cell with amorphous $Ge_2Sb_2Te_5$ chalcogenide and calculation results obtained from the coupled solution of Eqs. (2) and (6) for three values of the amorphous chalcogenide thickness, namely u_a=10, 25, and 40 nm. The three bias points P1, P2, and P3 considered in Fig. 5 are shown.

$$\frac{dE_F}{dz} = qF - \frac{qn_T}{J}\frac{E_F - E_{F0}}{\tau_{rel}}, \tag{6}$$

where the first and second terms on the right hand side describe energy gain and loss, respectively. Equation (6) has to be solved together with Eq. (2): in the latter, the equilibrium Fermi level E_{F0} has to be replaced by the more general quasi-Fermi level E_F, thus allowing to describe off-equilibrium conditions at threshold switching.

IV. SIMULATION RESULTS

Coupled Eqs. (2) and (6) and the relation between field and potential energy $F=q^{-1}dE'_C/dz$ were solved for any arbitrary current density J, thus obtaining the profiles of the quasi-Fermi level (E_F), of the electrostatic potential (E'_C) and the total voltage across the chalcogenide layer. Figure 6 shows the resulting theoretical *I-V* characteristic compared to experimental data for a phase-change memory device. This consists of a $Ge_2Sb_2Te_5$ layer with a constrained bottom contact with area of about 1000 nm^2, to enhance the current crowding and the consequent Joule heating, which is used for melting and crystallization processes.[24] The cell was measured after the application of a programming pulse with a quenching time of less than 20 ns, resulting in the formation of an amorphous region in the chalcogenide layer by quenching from the liquid phase. In the calculations, it was assumed that $E'_C - E_{F0}$=0.3 eV, Δz=7 nm, and $N_T=3\times10^{19}$ cm^{-3}. The energy relaxation time was assumed $\tau_{rel}=10^{-13}$ s, which agrees well with the rate of energy loss in amorphous semiconductors due to electron-phonon interaction.[23] A higher limit for the energy loss rate in amorphous semiconductors is approximated by Mott and Davis[20] as $dE/dt=-\hbar w_0^2$, leading to $\tau_{rel}\approx\Delta E/(\hbar w_0^2)\approx 1/w_0$ $=0.7\times10^{-13}$ s for $\hbar w_0$=10 meV. A longer relaxation time is expected for increasingly low density of trap states and high-energy distance between contiguous levels.[19]

In Fig. 6, different values for the thickness u_a of the amorphous region were assumed, and the best agreement with

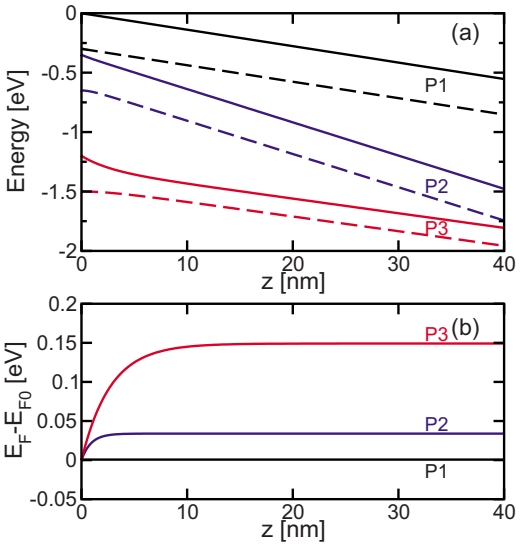

FIG. 7. (Color online) Calculated profiles of conduction-band mobility edge E'_C [solid line, (a)], quasi-Fermi level E_F [dashed line, (a)], and average excess energy E_F-E_{F0} (b), for the three bias points P1, P2, and P3 in Fig. 6. Thickness of the amorphous chalcogenide layer is u_a=40 nm.

experiments was obtained for u_a=40 nm, which is consistent with direct transmission electron microscopy (TEM) observation of the amorphous region in the memory cell.[25] The difference between the experimental and calculated *I-V* curves above the switching point is due to circuit-induced current spiking due to NDR[4,26] and consequent crystallization. As a result, the measured *I-V* characteristic above switching should not be taken as a reference for the electrical behavior of the amorphous-chalcogenide device.

To understand the switching mechanisms in this model, Fig. 7 shows the calculated profile of E'_C and E_F [Fig. 7(a)] and of E_F-E_{F0} [Fig. 7(b)] for u_a=40 nm at the three bias points shown in Fig. 6. These are chosen in the subthreshold regime (bias point P1 at a current $I=2\times10^{-7}$ A, where the differential resistance is positive or $dV/dI>0$), at the switching point (P2 at $I=5\times10^{-6}$ A, $dV/dI=0$) and above the switching point (P3 at $I=5\times10^{-5}$ A, $dV/dI<0$). Positive and negative electrodes in the simulations were assumed ideal conductors (zero resistivity) and the contacts were assumed ohmic.[19] In the subthreshold region (bias point P1), both E'_C and $E_F\approx E_{F0}$ are linear, indicating a uniform electric field and an equilibrium energy distribution of electrons. At the switching point P2, the E_F profile is significantly higher than E_{F0}. This is also clear from Fig. 7(b), showing that the excess energy E_F-E_{F0} increases linearly for very small z close to the cathode, then saturates to E_F-$E_{F0}\approx$30 meV for $z>3$ nm. This can be understood based on Eq. (6), where energy gain dominates over relaxation for z close to the cathode, yielding a linear increase $E_F=E_{F0}+qFz$. For large z, relaxation becomes relatively important and damps the excess energy to

$$E_F = E_{F0} + \frac{JF\tau_{rel}}{n_T}, \tag{7}$$

which accounts for the constant E_F-E_{F0} at large z in Fig. 7(b). Note that the excess energy is proportional to the power

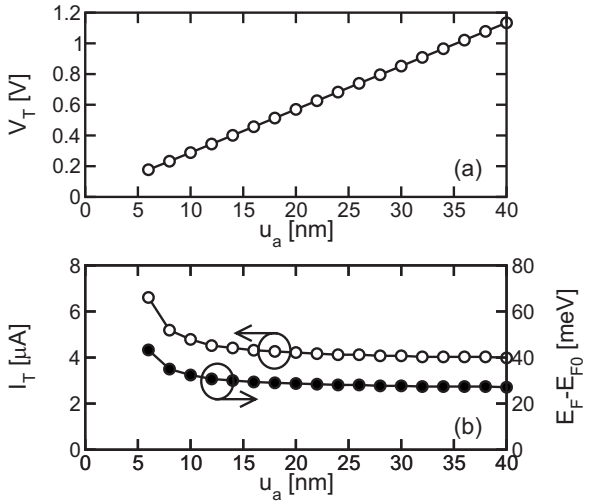

FIG. 8. Calculated V_T (a) and I_T (b) as a function of amorphous chalcogenide thickness u_a. Also shown is the excess energy in the ON region at switching E_F-E_{F0} (b).

density P'''=JF in Eq. (7), and can be viewed as the fraction of Joule power transferred to the electron population and not yet converted in lattice heating by the relaxation process. Equation (7) also applies to bias point P1, although the Joule power is negligible here and E_F-E_{F0} cannot be resolved in the figure.

The E'_C profile in the NDR region (bias point P3) becomes markedly nonuniform, with a large electric field close to the cathode interface and a small field for z sufficiently far from the cathode. This can be explained by the E_F-E_{F0} profile in Fig. 7(b), where the excess energy increases from 0 at the cathode interface (z=0) to a large value for $z>15$ nm (E_F-$E_{F0}\approx 0.15$ eV). Here, a relatively small field is needed to sustain the current density flowing in the device, since J depends exponentially on E_F in Eq. (2). As a result, the voltage in P3 is smaller than in P2, although the respective current is larger, which is the distinctive NDR feature of threshold switching. It can be concluded that switching in this model results from the increase in E_F and the collapse of F in the chalcogenide region far from the cathode interface, which will be called the ON region.[16]

Figure 8 shows the calculated threshold voltage V_T and threshold current I_T, defined as the coordinates of the point where dV/dI=0, as a function of u_a. V_T linearly increases with u_a in Fig. 8(a), in agreement with the reported critical field for threshold switching.[27] In Fig. 8(b), I_T is almost constant ($I_T\approx 4$ μA) for $u_a>10$ nm, which from Eq. (2), is consistent with a constant electric field at switching. However, for u_a decreasing below 10 nm, I_T increases. This can be understood considering the calculated E_F-E_{F0} in the ON region at the switching point V_T also shown in Fig. 8(b): For small u_a, the thickness of the ON region with saturated excess energy E_F-E_{F0} becomes increasingly small, thus the field collapse results in a smaller voltage snap back. Conversely, to establish the condition dV/dI=0, a larger excess energy is needed for increasingly small u_a. The larger I_T for small u_a is reflected by a weak increase in switching field V_T/u_a in Fig. 8(a), in agreement with experimental results as

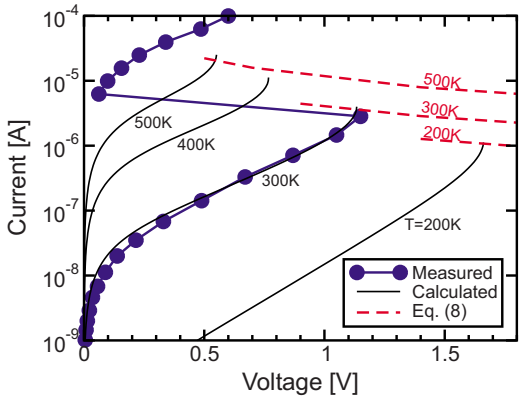

FIG. 9. (Color online) Calculated I-V characteristics for increasing temperature. Also shown is the constant-power locus of switching points according to Eq. (8). A critical power density $P'''_T = 10^{11}$ W cm^{-3} at 300 K is obtained from Eq. (8).

a function of the thickness of the amorphous chalcogenide layer.[24]

Figure 9 shows the calculated I-V characteristics for increasing T, from 200 to 500 K. The calculated curves are reported only in the subthreshold regime ($I<I_T$). The subthreshold current increases for increasing T, as a result of the strong temperature activation of hopping transport in Eq. (2). V_T decreases and I_T increases with T, which is consistent with previous experiments on chalcogenide glasses.[28,29] This can be explained noting that conductivity increases exponentially with $\gamma=(E_F$-$E_{F0})/$kT in Eq. (2). Switching occurs only when γ reaches a critical value γ_T in the ON region [$\gamma_T\approx 1$ from the E_F profile in Fig. 8(b)], thus causing the internal collapse of the electric field and initiating the NDR state. The critical value of γ_T can be translated into a *constant-power condition* for switching, with a critical power density P'''_T given by Eq. (7) as

$$P'''_T = \mathrm{JF} = \frac{\gamma_T N_T (\mathrm{kT})^2}{\tau_{\mathrm{rel}}(E'_C\text{-}E_{\mathrm{F0}})}, \tag{8}$$

where Eq. (5) was used. The validity of this criterion is demonstrated in Fig. 9, where switching points are found to lie very close to constant-power curves at their respective temperatures (e.g., $P'''_T=10^{11}$ W cm^{-3} for T=300 K).

The dependence of transport and switching processes on the mobility gap (hence on chemical composition) of the chalcogenide glass was finally investigated. Figure 10 shows calculated I-V curves for increasing E'_C-E_{F0}, in the range from 0.2 to 0.4 eV. While changing E'_C-E_{F0} has a dramatic impact on the subthreshold current, due to the exponential dependence in Eq. (2), I_T remains almost unaffected, as a result of the constant-power condition in Eq. (8). The mobility-gap dependence in Fig. 10 is in agreement with the relatively small threshold voltage observed in narrow-gap SbTe alloys[5] and with the composition dependence of V_T among pseudobinary compounds $(\mathrm{GeTe})_n(\mathrm{Sb_2Te_3})_m$.[30]

V. DISCUSSION

The physical interpretation and modeling of threshold switching in this work is based on the crucial role of energy

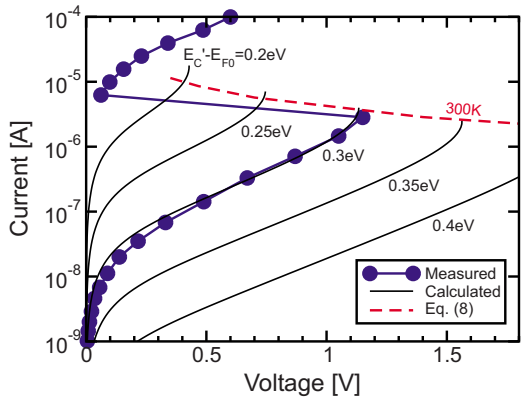

FIG. 10. (Color online) Calculated *I-V* characteristics for increasing energy difference E_C'-E_{F0} at room temperature. Also shown is the constant-power locus of switching points according to Eq. (8). A critical power density $P_T''' = 10^{11}$ W cm^{-3} is obtained from Eq. (8).

gain for the hopping process. Carrier energy gain in amorphous semiconductors (e.g., chalcogenide glasses), which results from the balance between field-driven gain and phonon-induced energy relaxation, is similar to the hot-electron effect in crystalline semiconductor (e.g., silicon). However, it should be remarked that the impact on the transport processes is rather different in the two cases. In fact, the energy gain of a localized electron exponentially enhances its hopping rate, or equivalently its velocity. This results from the thermal activation of the hopping process: Equation (2) predicts in fact a current increase by a factor e for an energy enhancement of a mere kT. In the case of crystalline semiconductor, instead, the drift and diffusion processes depend on carrier mobility, which is controlled by the effective mass and the scattering rate. While the former is rather insensitive of the carrier energy (except for intervalley scattering effects in GaAs, which degrades the effective mobility), the scattering rate strongly increases with energy due to optical phonon and impact ionization scattering effects. This leads to a general decrease in carrier mobility, as opposed to the conductivity enhancement for increasing energy, which is essential to account for the threshold-switching phenomenon.

It should be noted that the conductivity enhancement alone may not account for the NDR state and the threshold switching effect. The second basic ingredient which is necessary to explain the NDR behavior is the nonuniform profile of the electric field, which is established at the onset of threshold switching. The field distribution is nonuniform along the amorphous layer thickness because of the finite distance ("dead space") required for electrons to gain energy, as evidenced by the calculated E_F-E_{F0} in Fig. 7. The elevated field in this dead space provides the necessary energy gain to sustain the large conductivity and the small electric field in the ON space above the switching point. Dead space effects are frequently encountered in crystalline-semiconductor devices based on hot carriers, such as avalanche photodiodes[31,32] and Gunn diodes.[33] Therefore, it is not surprising that a dead-space effect strongly influences threshold switching, which is intimately related to energy gain in localized states.

Finally, it should be noted that, due to the general hypothesis assumed in the development of this model, the threshold-switching theory discussed in this work may apply not only to chalcogenide glasses, but generally to most amorphous semiconductors featuring NDR and associated switching effect. In fact, according to the theoretical explanation in this work, switching results from two necessary conditions: (a) hopping conduction with a large concentration of localized states and a deep equilibrium Fermi level and (b) a finite energy relaxation rate. Thus this switching model may account for the observed switching effects in other semiconductors such as amorphous boron and transition-metal oxides.[11,29] On the other hand, the threshold-switching mechanism discussed in this work may be excluded for most crystalline and polycrystalline semiconductors, where the Fermi level is not necessarily deep (because of possible doping resulting from impurities or point defects) and/or the trap concentration is not sufficient for hopping to be the dominant transport mechanism, because of the lack of sufficient disorder.

VI. CONCLUSIONS

In conclusion, a threshold-switching mechanism and model based on the balance between electron energy gain and relaxation in the hopping transport have been presented. Threshold switching is explained by the collapse of the electric field in the chalcogenide material as a result of the off-equilibrium, high-energy distribution of trapped electrons. Threshold switching is shown to obey a critical electrical power-density condition. The proposed switching model allows predicting the subthreshold characteristics and threshold points for different thickness, temperature, and energy gap of the chalcogenide material, thus contributing to physics-based design and engineering of phase-change memory devices.

ACKNOWLEDGMENTS

The author would like to thank S. Lavizzari, U. Russo, M. Bernasconi, A. L. Lacaita, Y. Zhang, D. Kau, and G. Spadini for valuable discussions and suggestions.

*Fax+39 02 236 7604; ielmini@elet.polimi.it

[1] A. Kolobov, P. Fons, A. Frenkel, A. Ankudinov, J. Tominaga, and T. Uruga, Nat. Mater. **3**, 703 (2004).
[2] M. Wuttig, Nat. Mater. **4**, 265 (2005).
[3] S. R. Ovshinsky, Phys. Rev. Lett. **21**, 1450 (1968).
[4] D. Ielmini, D. Mantegazza, A. L. Lacaita, A. Pirovano, and F. Pellizzer, IEEE Electron Device Lett. **26**, 799 (2005).
[5] M. Lankhorst, B. Ketelaars, and R. Wolters, Nat. Mater. **4**, 347

(2005).
[6] R. A. Street and N. F. Mott, Phys. Rev. Lett. **35**, 1293 (1975).
[7] N. F. Mott, in *Electrons in Glass*, Nobel Lectures, Physics 1971–1980, edited by S. Lundqvist (World Scientific, Singapore, 1992).
[8] S. R. Ovshinsky, Phys. Rev. Lett. **36**, 1469 (1976).
[9] D. Adler, H. K. Henisch, and N. Mott, Rev. Mod. Phys. **50**, 209 (1978).
[10] D. Adler, M. S. Shur, M. Silver, and S. R. Ovshinsky, J. Appl. Phys. **51**, 3289 (1980).
[11] D. Emin, Phys. Rev. B **74**, 035206 (2006).
[12] D. Emin, C. H. Seager, and R. K. Quinn, Phys. Rev. Lett. **28**, 813 (1972).
[13] C. H. Seager, D. Emin, and R. K. Quinn, Phys. Rev. B **8**, 4746 (1973).
[14] D. Emin, Philos. Mag. **35**, 1189 (1977).
[15] D. Ielmini and Y. Zhang, Appl. Phys. Lett. **90**, 192102 (2007).
[16] D. Ielmini and Y. Zhang, J. Appl. Phys. **102**, 054517 (2007).
[17] A. K. Jonscher, J. Phys. C **4**, 1331 (1971).
[18] A. K. Jonscher and C. K. Loh, J. Phys. C **4**, 1341 (1971).
[19] A. K. Jonscher and R. M. Hill, in *Electrical Conduction in Disordered Nonmetallic Films, Physics of Thin Films*, edited by G. Hass, M. H. Francombe, and R. W. Hoffman (Academic, New York, 1975), Vol. 8.
[20] N. F. Mott and E. A. Davis, *Electronic Processes in Non-Crystalline Materials* (Clarendon, Oxford, 1979).
[21] D. Ielmini, S. Lavizzari, D. Sharma, and A. L. Lacaita, Appl. Phys. Lett. **92**, 193511 (2008).
[22] N. K. Hindley, J. Non-Cryst. Solids **5**, 16 (1970).
[23] N. K. Hindley, J. Non-Cryst. Solids **5**, 31 (1970).
[24] D. Ielmini, A. L. Lacaita, A. Pirovano, F. Pellizzer, and R. Bez, IEEE Electron Device Lett. **25**, 507 (2004).
[25] K. Kim and S. J. Ahn, Proceedings of the International Reliability Physics Symposium (IRPS), 2005 (unpublished), p. 157.
[26] F.-J. Niedernostheide, H.-J. Schulze, S. Bose, A. Wacker, and E. Scholl, Phys. Rev. E **54**, 1253 (1996).
[27] W. D. Buckley and S. H. Holmberg, Phys. Rev. Lett. **32**, 1429 (1974).
[28] H. Fritzsche, IBM J. Res. Dev. **13**, 515 (1969).
[29] P. J. Walsh, R. Vogel, and E. J. Evans, Phys. Rev. **178**, 1274 (1969).
[30] X. S. Miao, L. P. Shi, H. K. Lee, J. M. Li, R. Zhao, P. K. Tan, K. G. Lim, H. X. Yang, and T. C. Chong, Jpn. J. Appl. Phys., Part 1 **45**, 3955 (2007).
[31] S. M. Sze, *Physics of Semiconductor Devices* (Wiley, New York, 1981).
[32] Y. Okuto and C. R. Crowell, Phys. Rev. B **10**, 4284 (1974).
[33] A. S. Spinelli, A. Pacelli, and A. L. Lacaita, Appl. Phys. Lett. **69**, 3707 (1996).